

Elastic scattering in the ${}^6,{}^7\text{Li} + {}^{80}\text{Se}$ systems

L. Fimiani,¹ J. M. Figueira,^{1,2} G. V. Martí,¹ J. E. Testoni,¹ A. J. Pacheco,^{1,2} W. H. Z. Cárdenas,¹ A. Arazi,^{1,2} O. A. Capurro,¹ M. A. Cardona,^{1,2,3} P. Carnelli,^{1,2,3} E. de Barbará,¹ D. Hojman,^{1,2} D. Martínez Heimann,^{1,2} and A. E. Negri^{1,2}

¹Laboratorio Tandem, Comisión Nacional de Energía Atómica, B1650KNA San Martín, Buenos Aires, Argentina

²Consejo Nacional de Investigaciones Científicas y Técnicas, C1033AAJ Ciudad de Buenos Aires, Argentina

³Escuela de Ciencia y Tecnología, Universidad de San Martín, B1650BWA San Martín, Buenos Aires, Argentina

(Received 26 April 2011; revised manuscript received 24 July 2012; published 8 October 2012)

Elastic-scattering angular distributions for the ${}^6,{}^7\text{Li} + {}^{80}\text{Se}$ systems were measured at center-of-mass energies from below to above the Coulomb barrier, $13 \leq E_{c.m.} \leq 24$ MeV. The experimental elastic-scattering cross sections were analyzed within the framework of the optical model to study the energy dependence of the real and imaginary parts of the nuclear-interaction potential. The main objective was to investigate the threshold anomaly in those weakly bound systems. The behavior of the calculated potentials as a function of energy indicates that our results are qualitatively consistent with the dispersion relation. The threshold anomaly was observed in the ${}^7\text{Li} + {}^{80}\text{Se}$ system and for the ${}^6\text{Li} + {}^{80}\text{Se}$ system a breakup threshold anomaly is apparent. An analysis of the absorptive processes, involved in the discussion of the experimental results, was performed using the phenomenological optical potentials that best fit the experimental data.

DOI: [10.1103/PhysRevC.86.044607](https://doi.org/10.1103/PhysRevC.86.044607)

PACS number(s): 25.70.Bc, 24.10.Ht, 25.70.Mn

I. INTRODUCTION

The production of radioactive beams has enabled the investigation of the dynamics and the structure of nuclei far from the valley of stability, and it has also made it possible to recreate nuclear reactions of astrophysics interest in the laboratory. When these exotic and/or unstable nuclei are used to induce nuclear reactions there exists in general a large probability of breakup, giving rise to interesting effects in comparison with the results obtained with tightly bound systems, in which breakup processes are less likely. Radioactive beams have very low intensities because they are obtained as secondary products of specific transfer and/or incomplete fusion reactions, thus making experiments very difficult and time consuming. For this reason the use of beams of the stable ${}^6\text{Li}$, ${}^7\text{Li}$, and ${}^9\text{Be}$ weakly bound nuclei to study the role played by the breakup channel has increasingly become a subject of interest in heavy-ion research [1–3]. The separation energies of α particles for the breakup of ${}^6\text{Li}$ and ${}^7\text{Li}$, and the neutron separation energy for the breakup of ${}^9\text{Be}$ into one neutron and two α particles, are $S_\alpha({}^6\text{Li}) = 1.47$ MeV, $S_\alpha({}^7\text{Li}) = 2.47$ MeV, and $S_n({}^9\text{Be}) = 1.67$ MeV, respectively.

The question of whether the occurrence of fusion is enhanced or hindered by the breakup channel has been addressed in Ref. [2] (and references therein) and Refs. [4–8]. The quasielastic scattering cross sections of weakly bound systems and their relation with the breakup channel have also attracted interest [9–13]. It has also been shown that the sequential breakup through the first resonant state of the ${}^6\text{Li}$ nucleus is an important channel to be included in coupled-channels calculations, even at deep sub-barrier energies [10]. The elastic scattering of weakly bound projectiles has also been investigated in order to study both the influence of the breakup channel on the total-fusion cross sections [14], and the dispersion relation [15–17] associated with the so called threshold anomaly (TA) [18]. Recently, many experiments were performed in order to study those effects through the

elastic scattering of those loosely bound nuclei on different targets (see a review in Ref. [19] and references therein).

The elastic scattering of tightly bound heavy-ions, such as ${}^{12}\text{C}$, ${}^{16}\text{O}$, and ${}^{32}\text{S}$ [20–24], has been exhaustively investigated and interpreted in terms of the optical model. For these systems the real and imaginary parts of the optical potential are known to have a peculiar behavior at bombarding energies close to the Coulomb barrier, named threshold anomaly. Briefly, at high incident energies both parts of the nuclear interaction potential are essentially independent of the energy. At the Coulomb-barrier energy the imaginary part suddenly decreases in magnitude as the bombarding energy decreases, while the real part increases up to a maximum value, and then decreases. Such behaviors of the real and imaginary parts of the optical potential are consistent with the dispersion relation, which manifests itself as a localized variation in the real part of the potential as the bombarding energy goes down towards the Coulomb barrier [18]. The TA has been associated with the coupling of the inelastic channels, which results in a rapidly varying attractive contribution to the potential [16–18].

Although in the case of tightly bound projectiles the TA is usually present [16], the elastic-scattering cross sections in the stable weakly bound systems ${}^6,{}^7\text{Li} + \text{target}$ and/or ${}^9\text{Be} + \text{target}$ do not allow us to establish definite conclusions. The study of elastic scattering in weakly bound systems and its analysis in terms of the TA are important to evaluate the role played by the breakup processes in these systems. For the case of weakly bound systems it has been theoretically predicted that the coupling of the breakup channels to the elastic channel produces a repulsive effective polarization potential that could inhibit the manifestation of the TA [2,14]. Mahaux *et al.* [17] already gave intuitive arguments that weakly bound nuclei will not display a TA [25]. For these systems Hussein *et al.* [26,27] proposed a new kind of anomaly, the so called breakup threshold anomaly (BTA). The coupling of the breakup channels to the elastic channel would be reflected as an increase of the imaginary part of the optical potential

as a function of decreasing energies close to the Coulomb barrier. Because of the dispersion relation, the behavior of the imaginary potential would be associated with a decrease in the intensity of the real part of the optical potential.

The published works devoted to the analysis of elastic-scattering cross sections of reactions induced by weakly bound projectiles, and the subsequent interpretation in terms of the TA or the BTA, provide different results which in some cases seem to be contradictory, mainly for the ${}^7\text{Li}$ elastic scattering. Several studies on the elastic scattering of ${}^6\text{Li}$ on ${}^{27}\text{Al}$ [28,29], ${}^{64}\text{Ni}$ [30], ${}^{64}\text{Zn}$ [31], ${}^{90}\text{Zr}$ [32], ${}^{138}\text{Ba}$ [33], ${}^{144}\text{Sm}$ [34], and ${}^{208}\text{Pb}$ [14] indicated that the results were compatible with the absence of the conventional TA. The results for some others systems are contradictory, as for ${}^{58}\text{Ni}$ [30,35,36] and ${}^{28}\text{Si}$ [37,38]. In the case of the elastic scattering of ${}^7\text{Li}$ on different targets, the conventional TA was identified on ${}^{59}\text{Co}$ [39], ${}^{138}\text{Ba}$ [33], and ${}^{208}\text{Pb}$ [14], and no hints of any kind of anomaly was found on ${}^{27}\text{Al}$ [40], ${}^{28}\text{Si}$ [41], ${}^{116}\text{Sn}$ [42], and ${}^{144}\text{Sm}$ [34].

The present work attempts to investigate the influence of the breakup processes of ${}^{6,7}\text{Li}$ projectiles on a relatively medium-mass target ${}^{80}\text{Se}$ ($Z = 34$, $N = 46$) through the study of the behavior of the optical potentials deduced from the experimental elastic-scattering cross sections. The target was chosen because it has an intermediate mass between ${}^{27}\text{Al}$ and ${}^{144}\text{Sm}$, and the elastic scattering of ${}^{6,7}\text{Li}$ on these targets had already been studied by our group (see Refs. [28,34,40]). A similar analysis is proposed here, which should allow one to compare the results of the three systems on an equal footing. Preliminary reports of this work were presented in Refs. [43–45]. The objective is to obtain the set of potentials that best describes the angular distributions. For these potentials we investigate the absorptive processes that take place in the external nuclear region and their dependence on the projectile.

In this paper Sec. II is devoted to describe the experimental setup and to present the experimental data. Section III is devoted to the different approaches of the theoretical analysis intended for the interpretation of the present results and, finally, Sec. IV summarizes the work, discusses the conclusions, and provides some suggestions for future works to be carried out on this subject.

II. EXPERIMENTAL SETUP AND RESULTS

The experimental elastic-scattering angular distributions were obtained at energies around the Coulomb barrier, V_{CB} , from $0.8V_{CB}$ up to $1.6V_{CB}$, and extend over a large angular range of 20° – 170° (center-of-mass frame) except at the highest energies where the angular range was progressively reduced. According to Ref. [46] the calculated values of V_{CB} in the center-of-mass system are 15.5 and 15.0 MeV, for the ${}^6\text{Li} + {}^{80}\text{Se}$ and ${}^7\text{Li} + {}^{80}\text{Se}$ systems, respectively. Beams of ${}^{6,7}\text{Li}$ were supplied by the 20 UD tandem accelerator TANDAR at Buenos Aires, with approximately 10 pA intensities. Targets of enriched (99.8%) selenium-80, $110 \mu\text{g}/\text{cm}^2$ thick, evaporated on $20\text{-}\mu\text{g}/\text{cm}^2$ -thick carbon foils, were placed at the center of a 80-cm-diameter scattering chamber. The detection system used for the measurements consisted of an array of eight surface-barrier detectors with an angular

separation of 5° between adjacent detectors. The collimators were slits that accurately define the entrance angle of each detector with uncertainties not greater than 0.5° and yield similar counting rates in each detector. The energy resolution (FWHM) of the detectors varied between 0.5% to 1.5%. These values were enough to separate in the recorded spectra the inelastic-excitation peaks of the target nucleus relative to the elastic-scattering peak; the energies of the two lowest excited states of ${}^{80}\text{Se}$ are 0.667 and 1.449 MeV.

The angular distributions were measured in steps of 2.5° , taking extreme care to minimize all sources of systematic uncertainties. A surface-barrier detector placed at a fixed angle of $15.0^\circ \pm 0.1^\circ$ or $23.0^\circ \pm 0.1^\circ$ was used for normalization purposes. A Faraday cup at the end of the beam line, far away from the target, was used to monitor and integrate the total charge delivered by the beam. In order to obtain accurate values of the solid angle for each detector, several measurements of the Rutherford scattering of ${}^6,7\text{Li}$ by a ${}^{197}\text{Au}$ thin target were carried out at all the incident energies. Additional details about the detector system and the data-acquisition system can be found in Ref. [47]. The absolute uncertainties of the cross sections ranged from 1% to 15%, except for those measured at $E_{c.m.} \geq 18$ MeV for ${}^6\text{Li}$ and $E_{c.m.} \geq 17.5$ MeV for ${}^7\text{Li}$, where the uncertainties reached values of 25% at the most backward angles. The contribution to the experimental uncertainties due to target contaminants (oxygen and carbon) in the nominal target thickness was estimated to be less than 1%. This is a consequence of the fact that their elastic peaks can be easily separated from the ${}^{6,7}\text{Li}$ ions scattered-elastic peaks from the Se target. The most important contribution from the inelastic-scattering channels comes from the first 2^+ ($E^* = 0.667$ MeV) excited state of the ${}^{80}\text{Se}$ nucleus. The corresponding peak could be well identified in most of the spectra. The first excited state of the ${}^7\text{Li}$ nucleus, at 0.478 MeV energy above the ground state, could not be separated from the elastic peak at almost all the bombarding energies, but

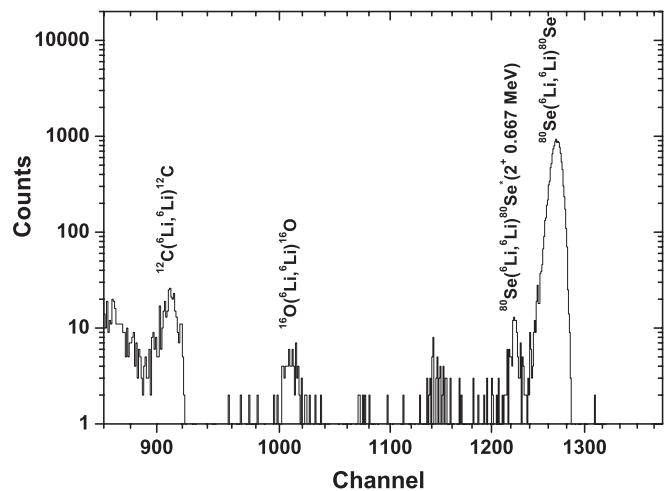


FIG. 1. Energy spectrum recorded for the elastic scattering of the ${}^6\text{Li} + {}^{80}\text{Se}$ system at $E_{lab} = 20$ MeV and at $\theta_{lab} = 50^\circ$. Different peaks corresponding to the elastic scattering of ${}^6\text{Li}$ from ${}^{16}\text{O}$ and ${}^{12}\text{C}$ (target contaminations) and the inelastic peak of the first excited state of the ${}^{80}\text{Se}$ nucleus are labeled.

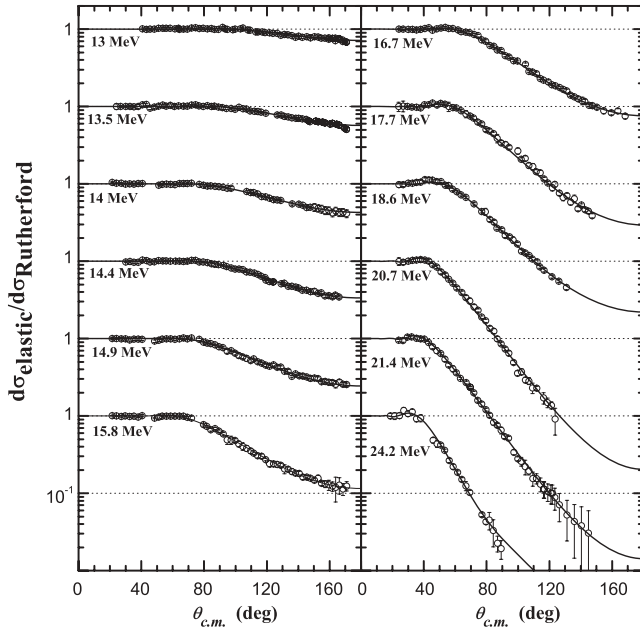


FIG. 2. Experimental elastic-scattering cross sections normalized to the Rutherford cross sections for the ${}^6\text{Li} + {}^{80}\text{Se}$ system (open circles) and their best fits from the phenomenological optical-model calculations (solid lines). Energies are given in the center-of-mass frame.

its contribution to the elastic-peak area was estimated to be less than 3% based on the analysis of the recorded spectra. As an example, Fig. 1 displays an energy spectrum recorded for the elastic scattering of the ${}^6\text{Li} + {}^{80}\text{Se}$ system at a

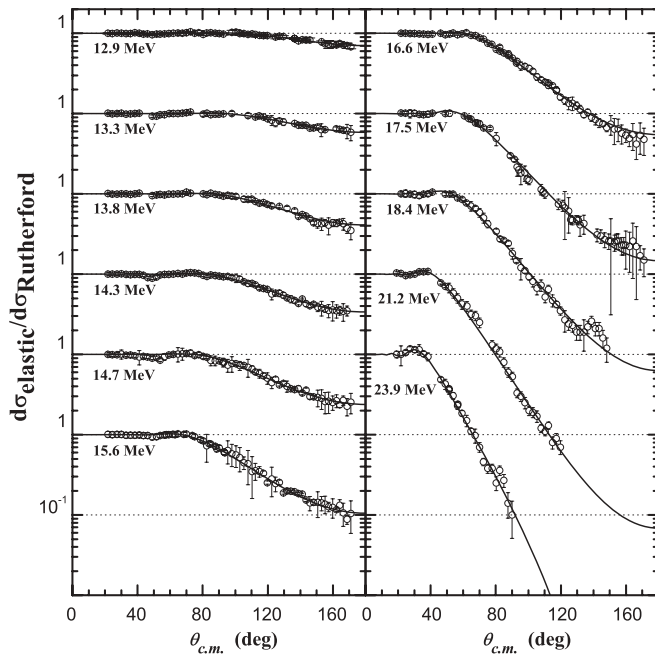


FIG. 3. Experimental elastic-scattering cross sections normalized to the Rutherford cross sections for the ${}^7\text{Li} + {}^{80}\text{Se}$ system (open circles) and their best fits from the phenomenological optical-model calculations (solid lines). Energies are given in the center-of-mass frame.

bombarding energy of 20 MeV and at a laboratory angle of 50° . The experimental angular distributions of the elastic-scattering cross sections normalized to Rutherford cross section and the best-fit curves obtained using the phenomenological potential (see the next section) are shown in Figs. 2 and 3 for ${}^6\text{Li} + {}^{80}\text{Se}$ and ${}^7\text{Li} + {}^{80}\text{Se}$ systems, respectively.

III. INTERPRETATION OF THE EXPERIMENTAL RESULTS

A. The phenomenological potential analysis

The standard phenomenological optical-model potential [48] is defined as

$$U(r) = V_C(r) - V f_V(r) - i W_{\text{vol}} f_{W_{\text{vol}}}(r) - i W_{\text{sup}} g_{W_{\text{sup}}}(r). \quad (1)$$

The first term of Eq. (1) represents the Coulomb potential of a uniformly charged sphere of radius R_C . The second term is the real nuclear potential, $V(r)$, and the third and fourth terms are a volume and a surface absorptive imaginary potential, $W_{\text{vol}}(r)$ and $W_{\text{sup}}(r)$ respectively. The parameters V , W_{vol} , and W_{sup} are the depths of the different contributions to the optical potential. The radial volume distributions are given by the expression

$$f_i(r) = \left[1 + \exp\left(\frac{r - R_i}{a_i}\right) \right]^{-1}, \quad (2)$$

where $R_i = r_i(A_p^{1/3} + A_t^{1/3})$ are the radii expressed in terms of the reduced-radius parameter r_i , A_p and A_t are the projectile and target mass numbers, and a_i are the diffusenesses. The index i stands for V and W_{vol} . The radial distribution of the imaginary surface potential is

$$g_{W_{\text{sup}}}(r) = -4a_{W_{\text{sup}}} df_{W_{\text{sup}}}(r)/dr. \quad (3)$$

The experimental angular-distribution data for the elastic scattering of the ${}^6,7\text{Li} + {}^{80}\text{Se}$ systems were analyzed, searching for sets of optical-model parameters that minimize the value of χ^2/point . The reduced radius $r_{W_{\text{sup}}}$ was selected in such a way that the maximum of the surface absorptive potential peaks at the position of the steepest variation of the real volume potential. The reduced-radius $r_{W_{\text{vol}}}$, and the diffuseness $a_{W_{\text{vol}}}$, were fixed at values lower than those of the real and surface imaginary components. Thus, the volume imaginary potential term that includes both parameters does not contribute significantly in the outer nuclear region.

The adopted values of the geometrical parameters were the same for both systems and their values are $r_{W_{\text{vol}}} = 1.0$ fm, $r_V = r_{W_{\text{sup}}} = 1.25$ fm, $a_{W_{\text{vol}}} = 0.3$ fm, and $a_V = a_{W_{\text{sup}}} = 0.75$ fm. The reduced radius for the Coulomb term was fixed at $r_C = 1.1$ fm. All the geometric parameters were kept fixed throughout the calculations, and the purpose of the analysis was to obtain the optical-potential strengths that best fit the experimental data. Initially the fitting procedure was carried out keeping as free parameters the depths of the real and the imaginary parts of the potentials, V , W_{vol} , and W_{sup} . The calculations based on the phenomenological potential were performed with the

TABLE I. The best optical-potential depths with their uncertainties for the different energies and reaction systems, obtained from the optical model χ^2 -minimization procedure performed on the measured elastic-scattering angular distributions. For both systems, the adopted volume imaginary potential parameters were $W_{\text{vol}} = 8.0$ MeV, $r_{W_{\text{vol}}} = 1.0$ fm, and $a_{W_{\text{vol}}} = 0.3$ fm, and the reduced radii and diffusenesses of the real and surface imaginary parts were $r_V = r_{W_{\text{sup}}} = 1.25$ fm and $a_V = a_{W_{\text{sup}}} = 0.75$ fm. The reduced radius for the Coulomb term is $r_C = 1.1$ fm.

${}^6\text{Li} + {}^{80}\text{Se}$						${}^7\text{Li} + {}^{80}\text{Se}$					
$E_{c.m.}$ (MeV)	V (MeV)	ΔV (MeV)	W_{sup} (MeV)	ΔW_{sup} (MeV)	χ^2/point	$E_{c.m.}$ (MeV)	V (MeV)	ΔV (MeV)	W_{sup} (MeV)	ΔW_{sup} (MeV)	χ^2/point
13.0	18.64	1.50	1.60	0.32	1.02	12.9	21.06	0.85	1.12	0.15	0.99
13.5	16.69	1.03	2.71	0.31	1.01	13.3	17.69	1.25	1.66	0.33	1.00
14.0	12.15	0.71	5.65	0.23	1.35	13.8	17.37	0.59	2.51	0.22	1.01
14.4	13.30	0.55	4.17	0.25	0.98	14.3	13.55	0.79	2.57	0.29	0.99
14.9	10.72	0.65	6.47	0.33	1.02	14.7	12.30	0.79	3.28	0.40	1.00
15.8	13.44	0.43	5.85	0.37	0.99	15.6	12.52	0.34	3.89	0.43	0.93
16.7	9.21	0.18	4.47	0.17	0.98	16.6	10.70	0.30	3.94	0.16	1.00
17.7	12.29	0.19	3.07	0.21	1.09	17.5	14.04	0.30	2.97	0.20	0.99
18.6	8.70	0.22	3.81	0.14	1.01	18.4	13.71	0.28	3.29	0.33	1.00
20.7	13.70	0.23	4.15	0.29	1.08	21.2	13.00	0.43	4.44	0.38	1.00
21.4	13.37	0.24	4.90	0.31	0.99	23.9	12.64	0.54	3.15	0.57	0.97
24.2	7.66	0.36	3.42	0.17	1.03						

code FRESKO [49] and their results will be presented in what follows.

In the first place it was observed that the depth W_{vol} could take values within a broad energy range without affecting essentially the goodness of the fit, especially at the lowest energies. For the rest of the analysis the value W_{vol} was kept fixed at $W_{\text{vol}} = 8$ MeV. Thus, the only two free parameters were the depths V and W_{sup} . The corresponding uncertainties have been evaluated considering variations of the

free parameters that produce an increase in one unit of χ^2 with respect to the minimum value [31,50,51]. Table I summarizes the results of this minimizing procedure.

The values of $W(R_M) = W_{\text{vol}}(R_M) + W_{\text{sup}}(R_M)$ and $V(R_M)$ calculated at the radius R_M (see below) as a function of the center-of-mass energy are shown in Figs. 4(a) and 4(b), respectively, for the ${}^6\text{Li} + {}^{80}\text{Se}$ system. The corresponding values for the ${}^7\text{Li} + {}^{80}\text{Se}$ system are displayed in Figs. 5(a) and

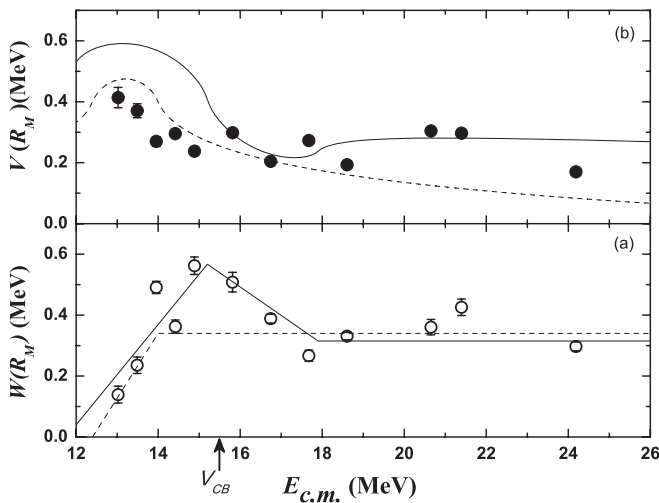


FIG. 4. (a) The imaginary potential (open circles) and (b) the real potential $V(R_M)$ (solid circles), as a function of the center-of-mass energy for the ${}^6\text{Li} + {}^{80}\text{Se}$ system. The lines in the bottom panel represent schematic segment fits to the imaginary potential $W(R_M)$. The dashed line assumes a TA-like behavior and the solid line a BTA-like behavior. The corresponding curves in the top panel represent the real potential $V(R_M)$ according to the dispersion-relation calculation. The potentials are calculated in the maximum-absorption radius $R_M = 10.5$ fm. The Coulomb-barrier energy is displayed as a vertical arrow.

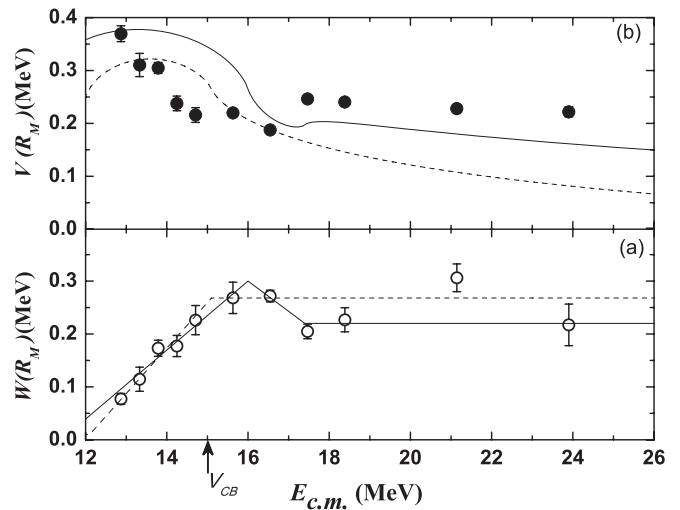


FIG. 5. (a) The imaginary potential (open circles) and (b) the real potential $V(R_M)$ (solid circles), as a function of the center-of-mass energy for the ${}^7\text{Li} + {}^{80}\text{Se}$ system. The lines in the bottom panel represent schematic segment fits to the imaginary potential $W(R_M)$. The dashed line assumes a TA-like behavior and the solid line a BTA-like behavior. The corresponding curves in the top panel represent the real potential $V(R_M)$ according to the dispersion-relation calculation. The potentials are calculated in the maximum-absorption radius $R_M = 10.9$ fm. The Coulomb-barrier energy is displayed as a vertical arrow.

5(b). In the present analysis, R_M is the maximum-absorption radius used as an equivalent of the strong-absorption radius concept referred in Refs. [16,22,52]. Their values have been found to be 10.5 fm for the ${}^6\text{Li} + {}^{80}\text{Se}$ system, and 10.9 fm for the ${}^7\text{Li} + {}^{80}\text{Se}$ system; these were obtained from Fig 8(a) (see Sec. III C). The curves in Figs. 4 and 5 represent theoretical estimates that will be explained later.

For ${}^6\text{Li} + {}^{80}\text{Se}$, the dependence of $W(R_M)$ on $E_{c.m.}$ [see Fig. 4(a)] can be qualitatively described as having an approximately constant value at the highest energies down to $E_{c.m.} = 18$ MeV (i.e. 2.5 MeV above the barrier). Below this energy $W(R_M)$ increases as the energy decreases to reach a maximum value at 15 MeV (about 0.5 MeV below the barrier) and finally it decreases and almost vanishes at the lowest measured energies. This particular energy dependence, more specifically, the fact that the absorption remains high even at sub-barrier energies, indicates that absorptive channels are still open in this region. According to Refs. [34,36] a serious candidate for these sub-barrier processes is the breakup of the weakly bound projectile. The observed overall behavior of $W(R_M)$ indicates a BTA-like energy dependence, which is rather similar to previous results of elastic scattering using the same weakly bound projectile [14,28–34,51], but the present data show a more important characteristic positive bump in the barrier region when comparing with the data of Ref. [34]. As far as the experimental real potential $V(R_M)$ is concerned [see Fig. 4(b)] the obtained values for this same system are approximately constant at energies above the barrier, whereas a slight monotonic rise can be observed below the barrier as the energy decreases.

A more quantitative understanding can be gained through the comparison of the experimental points with calculations that have been done under various assumptions. For this purpose we have applied the procedure used in Refs. [17,34], which describes the energy dependence of the imaginary optical potential by means of linear segments, and then calculates the corresponding real potential through the dispersion relation. Using this approach, the solid curve in Fig. 4(a) shows linear segments that reasonably describe the data points for ${}^6\text{Li} + {}^{80}\text{Se}$ under the assumption of a BTA-like behavior. The corresponding calculated values of $V(R_M)$ are represented by the solid curve in Fig. 4(b). The dashed curve in Fig. 4(a) shows a simpler (although less reasonable in this case) description of the imaginary potential, which assumes the characteristic behavior of the ordinary threshold anomaly; i.e., an approximately constant value of $W(R_M)$ above the barrier and a decrease as the energy falls below this value. The comparison between the two calculations of the real potential with the experimental values shows that, above the Coulomb barrier, the agreement is somewhat better for the solid curve (BTA) than for the dashed one (TA), reproducing the characteristic dip predicted by the BTA in the energy range between 15 and 18 MeV observed in the experimental data. Below the barrier both approaches show the expected bell shape, but the solid curve overestimates its magnitude. In summary, the whole analysis reinforces the interpretation that the phenomenological potential obtained for the ${}^6\text{Li} + {}^{80}\text{Se}$ system behaves in accordance with the breakup threshold anomaly.

A similar analysis has been done for the ${}^7\text{Li} + {}^{80}\text{Se}$ system, and the results are summarized in Fig. 5. Unlike the previous case, the behavior of the experimental $W(R_M)$ for this system [see Fig. 5(a)] is compatible with the occurrence of the TA; i.e., an almost constant value above the barrier and a rapid fall in the sub-barrier region. However, for this weakly bound system the absorption is still moderately present at sub-barrier energies, unlike what happens for the tightly bound systems where the absorption disappears close to the Coulomb barrier [34]. Near the barrier, a moderate increasing trend seems to exhibit a limited presence of open channels, but it comprises a short energy range that is supported for at most only two experimental points. The distribution of the $V(R_M)$ points in Fig. 5(b) can also be described by a constant value above the barrier. The rise observed at sub-barrier energies, as $E_{c.m.}$ decreases below the barrier, is somewhat more pronounced for this system than in the case of the ${}^6\text{Li}$ projectile.

The comparison with the theory has been done following a parallel procedure to that used for the previous system. The first of the calculations that have been done for ${}^7\text{Li} + {}^{80}\text{Se}$ (dashed curve) is representative of the experimental TA pattern observed in Fig. 5(a). The second calculation (solid curve) is based on a forced description of the same points assuming BTA. Although the agreement between the calculations and the experimental values of $V(R_M)$ in Fig. 5(b) is not totally satisfactory in any case, the fit seems to be qualitatively better for the dashed curve, in particular below the Coulomb barrier, thus lending additional support to the interpretation in terms of the ordinary threshold anomaly. The present results are in agreement with the results obtained in Refs. [14,33] where the usual TA was confirmed. They differ from those obtained for the ${}^7\text{Li} + {}^{27}\text{Al}$ [40] and ${}^7\text{Li} + {}^{144}\text{Sm}$ [34] systems using similar experimental and theoretical approaches, in which no threshold anomaly of any kind was observed.

The studies made based upon the phenomenological optical-model potentials reported in the present section can be complemented performing analyses that emphasize the role and the main characteristics of the involved absorption processes. This subject will be presented in Sec. III C.

B. The double-folding potential analysis

The elastic angular distributions for the ${}^6,7\text{Li} + {}^{80}\text{Se}$ systems were also analyzed using a microscopic double-folding potential $V_{DF}(r)$. This is important in order to test the consistency of the results that should be independent of the selected model [51]. For this potential Eqs. (10) and (19) of Ref. [53] were considered to describe the nucleon-nucleon interaction. The nuclear densities for the ${}^6\text{Li}$ and ${}^7\text{Li}$ projectiles were taken from Refs. [54] and [55], respectively, whereas for the target nucleus the systematization obtained from Chamon *et al.* [56] was adopted. In our analysis the potential V_{DF} has been calculated considering arbitrary fixed energies (those corresponding to the Coulomb barriers for each system) because the energy dependence is known to be very weak [53] or almost negligible within the range of interest for the present study [55]. To carry out the analysis presented here, the optical-model double-folding potential has the following

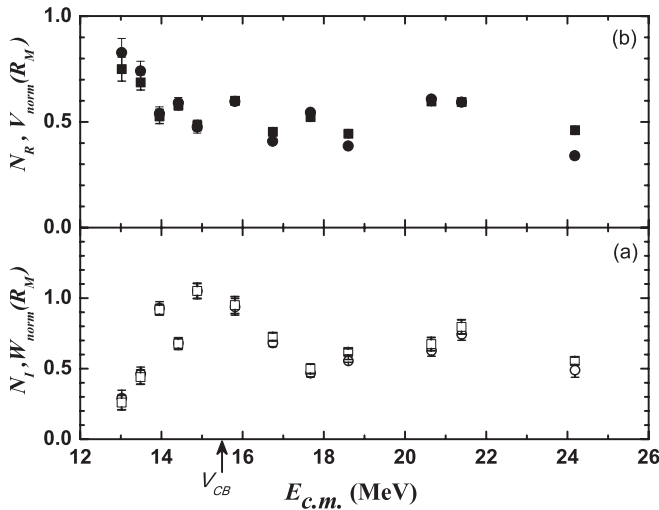


FIG. 6. Normalization factors of the (a) imaginary (open squares) and (b) real (solid squares) parts of the double-folding potential for the ${}^6\text{Li} + {}^{80}\text{Se}$ system as a function of the center-of-mass energy. Conveniently normalized values of the imaginary $W(R_M)$ and real $V(R_M)$ parts of the phenomenological potential denoted as $W_{\text{norm}}(R_M)$ (open circles) and $V_{\text{norm}}(R_M)$ (solid circles), respectively, have been included in order to compare with the corresponding double-folding normalization factors. The Coulomb-barrier energy is displayed as a vertical arrow.

form:

$$U(r) = V_C(r) - (N_R + iN_I)V_{DF}(r). \quad (4)$$

Here N_R and N_I are the normalization factors for the real and the imaginary parts of the nuclear potential, and they have been determined by fitting the experimental cross sections through a χ^2 -minimization procedure. The Coulomb potential was the same as that used in the phenomenological potential with a reduced radius $r_C = 1.1$ fm. The search of optimal parameters through the simultaneous fits of the angular distributions were carried out using the code FRESKO [49].

Figures 6 and 7 show, for both reaction systems, the behavior of the normalization factors N_R and N_I as a function of the center-of-mass energy (solid and open squares). For comparison, the values of $V(R_M)$ and $W(R_M)$ obtained in Sec. III A are also shown after a convenient normalization (solid and open circles). As expected there is a good agreement between both sets of parameters. A similar behavior for N_I was observed for ${}^6\text{Li} + {}^{90}\text{Zr}$ [32], ${}^6\text{Li} + {}^{58}\text{Ni}$ [36], and ${}^6\text{Li} + {}^{27}\text{Al}$ [28] although, for the present data, the decreasing trend of N_I below the barrier is well supported by several experimental points. For all these systems the conclusions would indicate the absence of the TA and/or the presence of the BTA.

In the case of ${}^7\text{Li} + {}^{80}\text{Se}$ system [see Fig. 7(a)] the present results regarding the dependence of N_I on $E_{c.m.}$ agree with those for the ${}^7\text{Li} + {}^{59}\text{Co}$ [39], ${}^7\text{Li} + {}^{138}\text{Ba}$ [33], and ${}^7\text{Li} + {}^{208}\text{Pb}$ [14], which have been interpreted in line with the conventional threshold anomaly.

In summary, the results presented in this section are consistent with the previous results presented in Sec. III A.

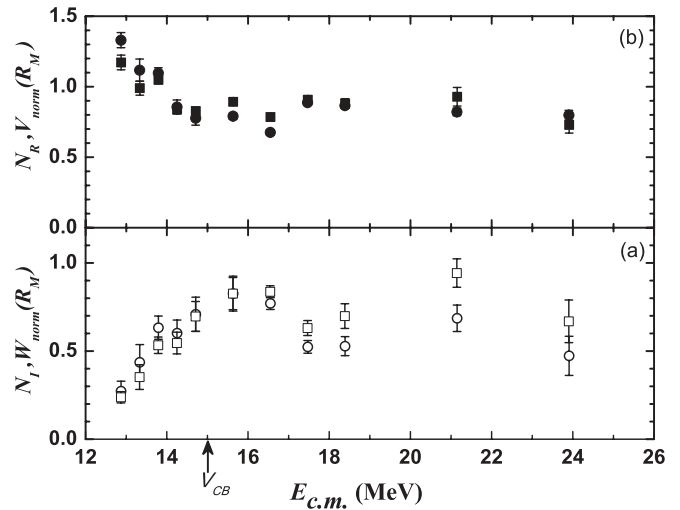


FIG. 7. Normalization factors of the (a) imaginary (open squares) and (b) real (solid squares) parts of the double-folding potential for the ${}^7\text{Li} + {}^{80}\text{Se}$ system as a function of the center-of-mass energy. Conveniently normalized values of the imaginary $W(R_M)$ and real $V(R_M)$ parts of the phenomenological potential denoted as $W_{\text{norm}}(R_M)$ (open circles) and $V_{\text{norm}}(R_M)$ (solid circles), respectively, have been included in order to compare with the corresponding double-folding normalization factors. The Coulomb-barrier energy is displayed as a vertical arrow.

C. The absorption in reactions induced by the projectiles ${}^6\text{Li}$ and ${}^7\text{Li}$

The results presented in the previous subsections regarding the behavior of the optical potentials as a function of energy, especially in the vicinity of the Coulomb barrier, have revealed differences between the two projectiles, ${}^6\text{Li}$ and ${}^7\text{Li}$. In what follows we will explore these differences focusing our analysis on the details of the absorptive processes that take place in those systems that involve weakly bound projectiles. For that purpose we will use, in the framework of the optical model, the potentials whose parameters were previously discussed in Sec. III A and are given in Table I.

This new approach addresses the subject, for both projectiles, in two steps. In the first one we analyze in detail the spatial distribution of the absorption processes at two specific energies. In a second step, we attempt a less detailed approach in the spatial distribution of the absorptive processes, but now including all the measured energies.

The first step is realized by means of two equivalent procedures:

1. analyzing the spatial contributions to the total-reaction cross section given by $\sigma_R^c(r)$, a continuous function of the radial coordinate;
2. studying the partial-reaction cross sections, σ_L , which are discrete functions of the orbital angular momentum L .

For the first procedure two representative energies are considered, one close to the Coulomb barriers ($E_{c.m.} = 13.77$ MeV) and the other well above them ($E_{c.m.} = 24.05$ MeV). These particular energy values are averages between the center-of-mass energies of each system that

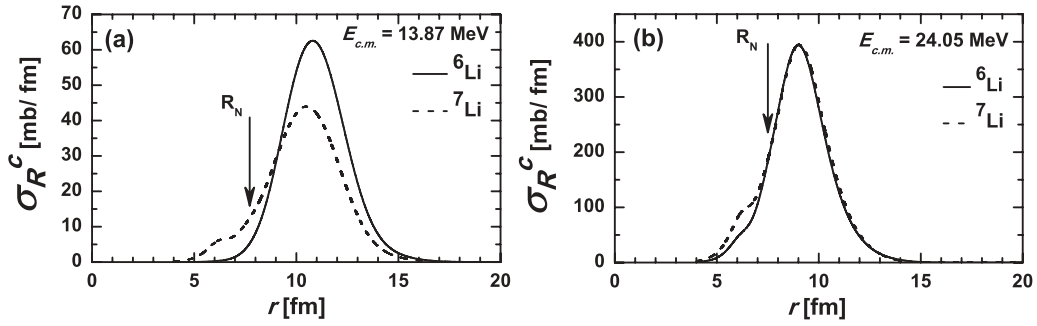


FIG. 8. The spatial density of absorption, corresponding to the ${}^6\text{Li} + {}^{80}\text{Se}$ (solid lines) and to the ${}^7\text{Li} + {}^{80}\text{Se}$ (dashed lines) systems, evaluated at the representative center-of-mass energies $E_{c.m.} = 13.87$ MeV [see panel (a)] and $E_{c.m.} = 24.05$ MeV [see panel (b)]. The arrows indicate the radius, $R_N = r_V(A_p^{1/3} + A_t^{1/3})$.

correspond to a single value of the laboratory energy. By taking this average we assume that the optical-potential parameters do not vary significantly within a small energy range, in this case 0.23 ± 0.06 MeV.

The methodology used in the present study is based on the evaluation of the diagonal matrix elements of the imaginary optical-model potential [57–60]. If $W(r)$ represents the imaginary optical potential and $\chi_L(r)$ are the partial wave functions with orbital angular momentum L , the total-reaction cross section may be expressed [61] as

$$\begin{aligned} \sigma_R &\equiv \int_0^\infty \sigma_R^c(r) dr \\ &= \int_0^\infty \left[-\frac{8\pi}{\hbar k^2 v} W(r) \sum_L (2L+1) |\chi_L(r)|^2 \right] dr \equiv \sum_L \sigma_L. \end{aligned} \quad (5)$$

Taking this expression as a reference, it is possible to evaluate quantities that will be later used in our analysis. One of these quantities is the spatial contribution to the total-reaction cross section $\sigma_R^c(r)$, which is shown in Fig. 8 as a function of the radial coordinate for the two representative energies.

It can be seen that, for both projectiles and both energies, the absorption occurs mainly in an outer region characterized by the condition $r > R_N$, with $R_N = r_V(A_p^{1/3} + A_t^{1/3})$. The values of R_N are 7.66 fm for the ${}^6\text{Li} + {}^{80}\text{Se}$ system and 7.78 fm for the ${}^7\text{Li} + {}^{80}\text{Se}$ system, respectively. At the energy close to the barrier [see Fig. 8(a)], the absorption in the outer region is significantly larger for ${}^6\text{Li}$ than for ${}^7\text{Li}$, while the opposite occurs in the inner region ($r < R_N$). At the energy well above the barrier [see Fig. 8(b)], the spatial distributions of the absorption for ${}^6\text{Li}$ and ${}^7\text{Li}$ are almost coincident in the outer region, whereas in the inner region ${}^7\text{Li}$ again prevails over ${}^6\text{Li}$. In addition, the comparison between Figs. 8(a) and 8(b) also shows that at higher energies the overall absorption increases considerably and the absorption peak shifts towards lower radial values. Both facts can be qualitatively understood in terms of an increasing degree of nuclear overlap as the energy increases. Although we have presented only the results for two representative energies, this analysis has been applied to the whole range of energies and the behavior of the absorption has been found to evolve smoothly from the low-energy to the high-energy regime.

The second procedure addresses the previous comparison between the behaviors of ${}^6\text{Li}$ and ${}^7\text{Li}$ projectiles from a slightly different viewpoint. Although equivalent to the previous one, it is based on the study of the partial-reaction cross section σ_L , a quantity implicitly defined in Eq. (5), as a function of the orbital angular momentum L .

The results of this complementary analysis are summarized in Fig. 9, which shows the values of σ_L (solid squares) together with the discriminated contributions of the outer region (open triangles) and of the inner region (open circles). These outer and inner contributions to σ_L are obtained considering partial integration ranges of the radial variable, i.e., from R_N to infinity in the first case and from the origin to R_N in the second one. The top (bottom) panels of this figure correspond to the low (high) bombarding energy whereas the left (right) panels correspond to the ${}^6\text{Li}$ (${}^7\text{Li}$) projectile.

The analysis of Fig. 9 shows that at both energies and for both projectiles the L distribution of the external absorption extends up to higher L values in comparison with the internal absorption. At the high energy (bottom panels) the L distributions of the absorption are very similar for the two projectiles, not only in the overall values but also in the discriminated internal and external contributions. In particular, we have also verified that the small shift of approximately $2\hbar$ towards higher L values in the case of ${}^7\text{Li}$ with respect to ${}^6\text{Li}$ can be explained by the mass differences.

Most important divergences between the two projectiles take place at the energy close to the barriers (top panels). In fact, at this low energy the contribution to the absorption that comes from the outer region is significantly larger for ${}^6\text{Li}$ than for ${}^7\text{Li}$ (as could also be expected from the radial distributions shown in Fig. 8). Due to differences in their shapes, this fact is not immediately apparent from a merely visual inspection of the L distributions themselves, but it is noticeable if one considers the sum $\sum_L \sigma_L(r > R_N)$, which takes quite different values at 13.87 MeV (231.0 mb for ${}^6\text{Li}$ and 173.9 mb for ${}^7\text{Li}$) and very similar values at 24.05 MeV (1104 mb for ${}^6\text{Li}$ and 1096 mb for ${}^7\text{Li}$).

The absorption that originates in the inner region has the opposite behavior, i.e., $\sigma_L(r < R_N)$ is larger for ${}^7\text{Li}$ than for ${}^6\text{Li}$ at both energies, and again the difference is much more pronounced at the near-barrier energy. Besides the comparison between projectiles, it may also be worth pointing out that, in

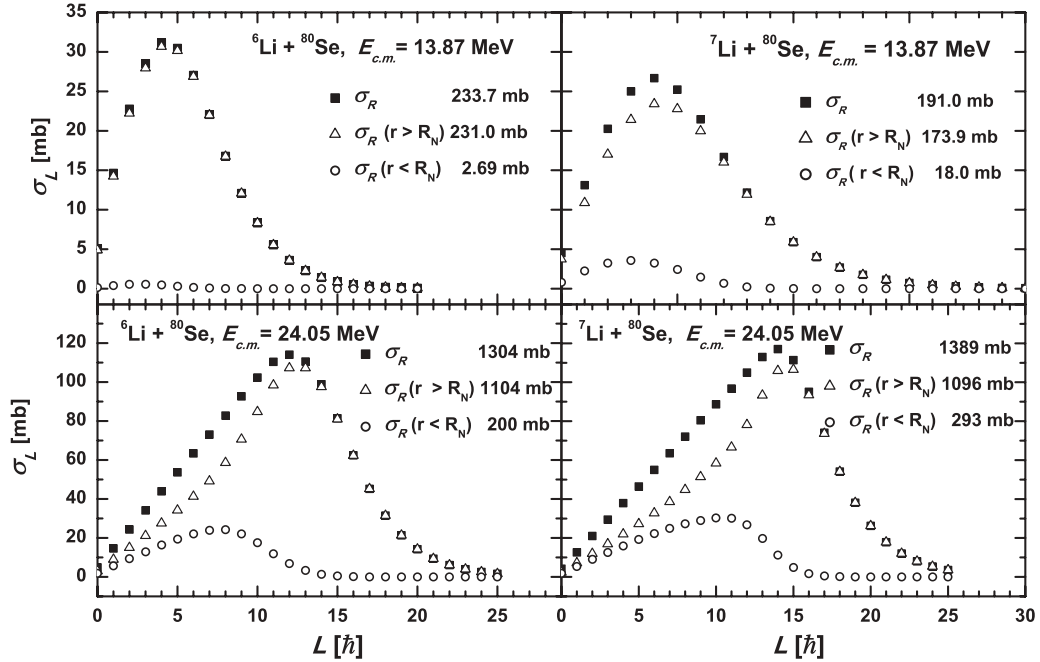


FIG. 9. Partial-reaction cross sections for the ${}^6\text{Li}$ and ${}^7\text{Li}$ projectiles at representative energies are plotted as a function of the orbital angular momentum, L , (solid squares). The contributions of the inner ($r < R_N$) (open circles) and outer ($r > R_N$) (open triangles) regions are discriminated. The top panels show the calculated data for ${}^6\text{Li}$ (left) and ${}^7\text{Li}$ (right) evaluated at the low-energy value of $E_{c.m.} = 13.87$ MeV. The bottom panels show the calculated data evaluated at the high-energy value of $E_{c.m.} = 24.05$ MeV.

the high-energy case, the linear behavior of σ_L (solid squares in Fig. 9) as a function of the orbital angular momenta up to about $L = 12\hbar$ for ${}^6\text{Li}$ and $L = 14\hbar$ for ${}^7\text{Li}$ indicates a complete absorption of the corresponding incident flux.

After the previous detailed analysis of absorption processes for the two extreme energies, in terms of the spatial and

angular-momentum distributions, let us return to the second step mentioned at the beginning of this section.

The comparative behavior of the total-reaction cross sections and the contributions of the inner and outer regions have finally been analyzed as a function of the center-of-mass energy for all the measured energies. The results are summarized in Fig. 10, which shows absolute values of the reaction cross sections. Although from this figure it is possible in principle to follow the complete evolution of both reaction systems as a function of the energy, it is useful to recast the results in a more significant way. For that purpose and in order to remove trivial geometrical and size factors, we define the reduced cross section according to Ref. [62],

$$\sigma_{R,\text{red}} = \frac{\sigma_R}{(A_p^{1/3} + A_t^{1/3})^2}. \quad (6)$$

These new quantities are used to define their relative difference $\Delta\sigma$ to evaluate (as a percentage) the enhancement of ${}^6\text{Li}$ over ${}^7\text{Li}$:

$$\Delta\sigma[\%] = \frac{(\sigma_{R,\text{red}}^{6\text{Li}} - \sigma_{R,\text{red}}^{7\text{Li}})}{(\sigma_{R,\text{red}}^{6\text{Li}} + \sigma_{R,\text{red}}^{7\text{Li}})} \times 200. \quad (7)$$

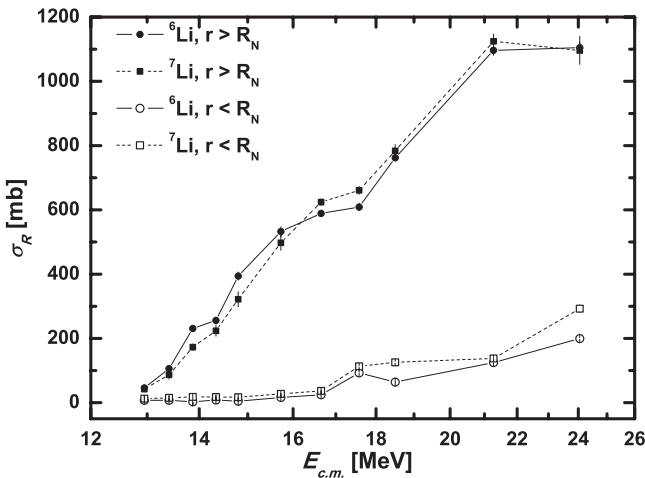


FIG. 10. Total-reaction cross sections as a function of the center-of-mass energy, for both projectiles and spatial regions, are represented as solid circles for the ${}^6\text{Li}$ projectile at the outer region ($r > R_N$), and open circles at the inner region ($r < R_N$). In the case of the ${}^7\text{Li}$ projectile, solid squares correspond to the outer region, and open squares to the inner region. The dashed and solid lines connecting the points are intended to guide the eye.

Figure 11 shows the dependence of $\Delta\sigma$ as a function of the center-of-mass energy for the outer region [panel (a)] and for the inner region [panel (b)]. The uncertainties shown in Fig. 10 as well as in Fig. 11 have been obtained, taking into account the errors of the optical parameters V and W_{sup} given in Table I.

From Fig. 11(a) it can be concluded that at sub-barrier energies the absorption in the external region (which has

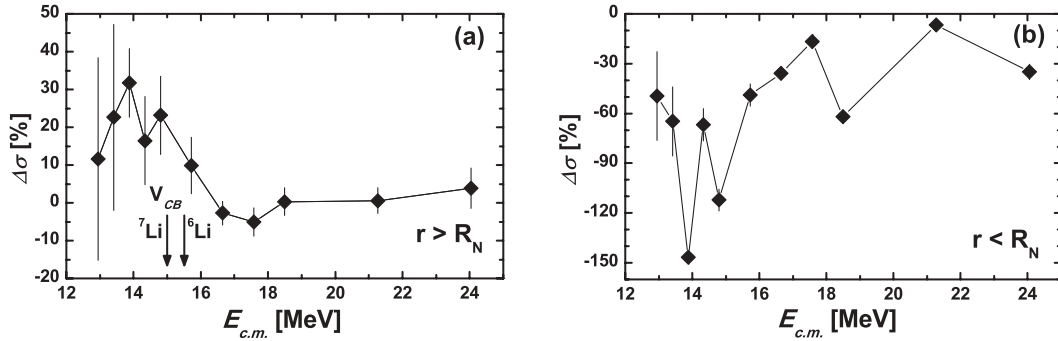


FIG. 11. (a) Percentage difference of the total-reaction cross sections, $\Delta\sigma$, between ${}^6\text{Li} + {}^{80}\text{Se}$ and ${}^7\text{Li} + {}^{80}\text{Se}$ systems as a function of the center-of-mass energy for the outer region, $r > R_N$; (b) as in panel (a) but for the inner region, $r < R_N$. The Coulomb barriers of the systems are indicated with arrows. The solid line connecting the points is intended to guide the eye.

already been shown to be the dominant contribution for these systems) is much larger for ${}^6\text{Li}$ than for ${}^7\text{Li}$. At energies just above the barriers the relative difference $\Delta\sigma$ decreases sharply, and as the energy increases it takes values that are small but still positive. From Fig. 11(b) it can be seen that the less important contribution to the absorption that originates in the inner region qualitatively has the opposite behavior. In fact, even if one disregards the fluctuations that are present in this case, the values of $\Delta\sigma$ are negative, i.e., the absorption is larger for ${}^7\text{Li}$ than for ${}^6\text{Li}$ in the whole energy range, especially near the barrier [see also Fig. 8(a)].

It is worth noticing that the analysis that has just been presented and summarized in Figs. 8 to 11 supports, from a different point of view, the conclusions regarding the behavior of the parameter $W(R_M)$ as a function of the bombarding energy that had been previously drawn in Sec. III A. In fact, the contrast between (i) the BTA for ${}^6\text{Li}$ shown in Fig. 4(a) (characterized by an increase of $W(R_M)$ as the energy decreases approaching the barrier and the persistence of these relatively high values even at moderately sub-barrier energies), and (ii) an almost ordinary TA-like behavior for ${}^7\text{Li}$ observed in Fig. 5(a) is consistent with the difference in absorptions for both systems reported in the present subsection. In particular, it is in agreement with the observation in Fig. 11(a) of a positive bump in the values of $\Delta\sigma$ for the external region at near-barrier energies.

The approach used in this subsection emphasizes the fact that the correct description of the experimental results involving the weakly bound projectiles ${}^6\text{Li}$ and ${}^7\text{Li}$ consistently requires the presence of an important peripheral absorption.

IV. SUMMARY AND CONCLUSIONS

We have measured elastic-scattering angular distributions for the ${}^{6,7}\text{Li} + {}^{80}\text{Se}$ systems at several bombarding energies from below to well above the Coulomb barrier. The experimental data have been analyzed using the optical model with a phenomenological Woods-Saxon shaped potential and a double-folding potential. The relevant parameters that best fit the elastic-scattering cross sections were obtained through a χ^2 -minimization procedure.

For the ${}^6\text{Li} + {}^{80}\text{Se}$ system the behavior of the imaginary part of the phenomenological potential and the imaginary normalization factor of the double-folding potential as a function of energy indicate the presence of the breakup threshold anomaly. For the ${}^7\text{Li} + {}^{80}\text{Se}$ system the behavior of the corresponding parts of the potential as a function of energy is consistent with a situation close to the ordinary threshold anomaly observed in tightly bound nuclei.

The observed differences between the elastic scattering of ${}^6\text{Li}$ and that of ${}^7\text{Li}$ on the same target can be attributed to several reasons. One of them is the difference in the nuclear structure of the two Li isotopes, which is negligible at high energies but becomes important in near and sub-barrier energy regimes [33]. Another reason can be related to the different breakup threshold energies, lower in the case of ${}^6\text{Li}$, and therefore producing for this projectile enhanced breakup probabilities mainly in the low-energy regime [51].

The absence of the threshold anomaly for the ${}^6\text{Li}$ -induced reactions was interpreted as evidence of the influence of the breakup process. Assumed to be the dominant direct reaction channel [33], it generates a weak coupling between elastic and inelastic or transfer channels and a strong coupling of the elastic channel to the continuum breakup states [28]. This coupling produces a repulsive polarization potential which is dominant, thus leading to the breakup threshold anomaly [28].

The presence of the threshold anomaly for the ${}^7\text{Li}$ elastic scattering has been ascribed to the strong couplings with the first excited states of the ${}^7\text{Li}$ inelastic channel [31,33]. In fact, there is a strong competition between the repulsive breakup polarization potential [63] and the attractive polarization potential produced by its first excited bound state [64]. These couplings produce a strong attractive polarization potential whose strength is larger than the repulsive polarization potential strength due to the breakup. The relevance of the breakup channel relative to other reaction channels can be accurately evaluated by means of continuous discretized coupled-channel calculations.

The differences between both projectiles have been further analyzed and found to be consistent with the results obtained through a detailed study of the absorption process and its dependence upon the radial coordinate and the angular momentum of the projectile-target relative motion. In particular,

the analysis of the absorptive imaginary potential lends support to the presence of the threshold anomaly in the case of ${}^7\text{Li}$ and the breakup threshold anomaly in the case of ${}^6\text{Li}$. Besides reinforcing our previous findings, this study performed in the framework of the optical model shows that the absorptive processes seems to be dominant in the outer region of the nuclear systems, i.e., at values of the radial coordinate that are somewhat larger than the radius of the real potential; however, as expected, closer to this radius in the case of the higher energies.

The results of the present study about the absorption processes in the case of weakly bound projectiles has aroused the interest to carry out similar analyses in the case of tightly bound projectiles.

ACKNOWLEDGMENTS

Some of us acknowledge the financial support of CONICET, CNEA, and MinCyT.

-
- [1] D. G. Baur, F. Rosel, and R. Shyam, *Phys. Rep.* **111**, 333 (1984).
- [2] L. F. Canto, P. R. S. Gomes, R. Donangelo, and M. S. Hussein, *Phys. Rep.* **424**, 1 (2006).
- [3] D. Martinez Heimann, A. J. Pacheco, A. Arazi, O. A. Capurro, P. Carnelli, D. S. Monteiro, J. O. Fernández Niello, J. M. Figueira, L. Fimiani, P. Grinberg *et al.*, in *Proceedings of International Conference on New Aspects of Heavy Ion Collisions Near the Coulomb Barrier (Fusion08), Chicago, 2008*, AIP Conf. Proc. No. 1098 (AIP, New York, 2009), p. 275.
- [4] D. J. Hinde, M. Dasgupta, B. R. Fulton, C. R. Morton, R. J. Wooliscroft, A. C. Berriman, and K. Hagino, *Phys. Rev. Lett.* **89**, 272701 (2002).
- [5] P. R. S. Gomes, I. Padron, M. D. Rodríguez, G. V. Martí, R. M. Anjos, J. Lubian, R. Veiga, R. Liguori Neto, E. Crema, N. Added *et al.*, *Phys. Lett. B* **601**, 20 (2004).
- [6] P. R. S. Gomes, M. D. Rodríguez, G. V. Martí, I. Padron, L. C. Chamon, J. O. Fernández Niello, O. A. Capurro, A. J. Pacheco, J. E. Testoni, A. Arazi *et al.*, *Phys. Rev. C* **71**, 034608 (2005).
- [7] P. K. Rath, S. Santra, N. L. Singh, R. Tripathi, V. V. Parkar, B. K. Nayak, K. Mahata, R. Palit, S. Kumar, S. Mukherjee *et al.*, *Phys. Rev. C* **79**, 051601 (2009).
- [8] P. R. S. Gomes, J. Lubian, B. Paes, V. N. Garcia, D. S. Monteiro, I. Padrón, J. M. Figueira, A. Arazi, O. A. Capurro, L. Fimiani *et al.*, *Nucl. Phys. A* **828**, 233 (2009).
- [9] H. M. Jia, C. J. Lin, H. Q. Zhang, Z. H. Liu, N. Yu, F. Yang, F. Jia, X. X. Xu, Z. D. Wu, S. T. Zhang *et al.*, *Phys. Rev. C* **82**, 027602 (2010).
- [10] D. S. Monteiro, O. A. Capurro, A. Arazi, J. O. Fernández Niello, J. M. Figueira, G. V. Martí, D. Martinez Heimann, A. E. Negri, A. J. Pacheco, V. Guimarães *et al.*, *Phys. Rev. C* **79**, 014601 (2009).
- [11] S. Mukherjee, B. K. Nayak, D. S. Monteiro, J. Lubian, P. R. S. Gomes, S. Appannababu, and R. K. Choudhury, *Phys. Rev. C* **80**, 014607 (2009).
- [12] D. R. Otomar, J. Lubian, P. R. S. Gomes, D. S. Monteiro, O. A. Capurro, A. Arazi, J. O. F. Niello, J. M. Figueira, G. V. Martí, D. M. Heimann *et al.*, *Phys. Rev. C* **80**, 034614 (2009).
- [13] V. I. Zagrebaev, *Phys. Rev. C* **78**, 047602 (2008).
- [14] N. Keeley, S. J. Bennett, N. M. Clarke, B. R. Fulton, G. Tungate, P. V. Drumm, M. A. Nagarajan, and J. S. Lilley, *Nucl. Phys. A* **571**, 326 (1994).
- [15] J. S. Toll, *Phys. Rev.* **104**, 1760 (1956).
- [16] M. A. Nagarajan, C. C. Mahaux, and G. R. Satchler, *Phys. Rev. Lett.* **54**, 1136 (1985).
- [17] C. Mahaux, H. Ngô, and G. R. Satchler, *Nucl. Phys. A* **449**, 354 (1986).
- [18] G. R. Satchler, *Phys. Rep.* **199**, 147 (1991).
- [19] A. DiPietro, *J. Phys.: Conf. Ser.* **205**, 012042 (2010).
- [20] A. Baeza, B. Bilwes, R. Bilwes, J. Diaz, and J. Ferrero, *Nucl. Phys. A* **419**, 412 (1984).
- [21] B. R. Fulton, D. W. Banes, J. S. Lilley, M. A. Nagarajan, and I. J. Thompson, *Phys. Lett. B* **162**, 55 (1985).
- [22] J. S. Lilley, B. R. Fulton, M. A. Nagarajan, and I. J. Thompson, *Phys. Lett. B* **151**, 181 (1985).
- [23] D. Abriola, D. DiGregorio, J. E. Testoni, A. Etchegoyen, M. C. Etchegoyen, J. O. Fernández Niello, A. M. J. Ferrero, S. Gil, A. O. Macchiavelli, A. J. Pacheco *et al.*, *Phys. Rev. C* **39**, 546 (1989).
- [24] D. Abriola, A. A. Sonzogni, M. di Tada, A. Etchegoyen, M. C. Etchegoyen, J. O. Fernández Niello, S. Gil, A. O. Macchiavelli, A. J. Pacheco, R. Piegaia *et al.*, *Phys. Rev. C* **46**, 244 (1992).
- [25] M. A. Tiede, D. E. Trcka, and K. W. Kemper, *Phys. Rev. C* **44**, 1698 (1991).
- [26] M. S. Hussein, P. R. S. Gomes, J. Lubian, and L. C. Chamon, *Phys. Rev. C* **73**, 044610 (2006).
- [27] M. S. Hussein, P. R. S. Gomes, J. Lubian, and L. C. Chamon, *Phys. Rev. C* **76**, 019902(E) (2007).
- [28] J. M. Figueira, J. O. Fernández Niello, D. Abriola, A. Arazi, O. A. Capurro, E. de Barbará, G. V. Martí, D. Martinez Heimann, A. E. Negri, A. J. Pacheco *et al.*, *Phys. Rev. C* **75**, 017602 (2007).
- [29] J. Fernández Niello, J. Figueira, D. Abriola, A. Arazi, O. Capurro, G. Martí, D. Martinez Heimann, A. Pacheco, E. de Barbará, I. Padrón *et al.*, *Nucl. Phys. A* **787**, 484 (2007).
- [30] M. Biswas, S. Roy, M. Sinha, M. K. Pradhan, A. Mukherjee, P. Basu, H. Majumdar, K. Ramachandran, and A. Shrivastava, *Nucl. Phys. A* **802**, 67 (2008).
- [31] M. Zadro, P. Figuera, A. D. Pietro, F. Amorini, M. Fisichella, O. Goryunov, M. Lattuada, C. Maiolino, A. Musumarra, V. Ostashko *et al.*, *Phys. Rev. C* **80**, 064610 (2009).
- [32] H. Kumawat, V. Jha, B. J. Roy, V. V. Parkar, S. Santra, V. Kumar, D. Dutta, P. Shukla, L. M. Pant, A. K. Mohanty *et al.*, *Phys. Rev. C* **78**, 044617 (2008).
- [33] A. M. M. Maciel, P. R. S. Gomes, J. Lubian, R. M. Anjos, R. Cabezas, G. M. Santos, C. Muri, S. B. Moraes, R. Liguori Neto, N. Added *et al.*, *Phys. Rev. C* **59**, 2103 (1999).
- [34] J. M. Figueira, J. O. F. Niello, A. Arazi, O. A. Capurro, P. Carnelli, L. Fimiani, G. V. Martí, D. M. Heimann, A. E. Negri, A. J. Pacheco *et al.*, *Phys. Rev. C* **81**, 024613 (2010).
- [35] E. F. Aguilera, E. Martinez-Quiroz, D. Lizcano, A. Gómez-Camacho, J. J. Kolata, L. O. Lamm, V. Guimaraes, R. Lichtenthäler, O. Camargo, F. D. Becchetti *et al.*, *Phys. Rev. C* **79**, 021601(R) (2009).
- [36] A. Camacho, E. F. Aguilera, E. M. Quiroz, P. R. S. Gomes, J. Lubian, and L. F. Canto, *Nucl. Phys. A* **833**, 156 (2010).

- [37] A. Pakou, N. Alamanos, A. Lagoyannis, A. Gillibert, E. C. Pollacco, P. A. Assimakopoulos, G. Doukelis, K. G. Ioannides, D. Karadimos, D. Karamanis *et al.*, *Phys. Lett. B* **556**, 21 (2003).
- [38] A. Gómez Camacho, P. R. S. Gomes, and J. Lubian, *Phys. Rev. C* **82**, 067601 (2010).
- [39] F. A. Souza, L. A. S. Leal, N. Carlin, M. G. Munhoz, R. Liguori Neto, M. M. de Moura, A. A. P. Suaide, E. M. Szanto, A. Szanto de Toledo, and J. Takahashi, *Phys. Rev. C* **75**, 044601 (2007).
- [40] J. M. Figueira, D. Abriola, J. O. Fernández Niello, A. Arazi, O. A. Capurro, E. de Barbara, G. V. Martí, D. Martinez Heimann, A. J. Pacheco, J. E. Testoni *et al.*, *Phys. Rev. C* **73**, 054603 (2006).
- [41] A. Pakou, N. Alamanos, G. Doukelis, A. Gillibert, G. Kalyva, M. Kokkoris, S. Kossionides, A. Lagoyannis, A. Musumarra, C. Papachristodoulou *et al.*, *Phys. Rev. C* **69**, 054602 (2004).
- [42] N. N. Deshmukh, S. Mukherjee, B. K. Nayak, D. C. Biswas, S. Santra, S. Appannababu, E. T. Mirgule, A. Saxena, D. Patel, R. K. Choudhury *et al.*, in *Proceedings of the IX Latin American Symposium on Nuclear Physics and Applications*, AIP Conf. Proc. No. 1423 (AIP, New York, 2012), p. 122.
- [43] L. Fimiani, G. V. Martí, A. Arazi, O. A. Capurro, M. A. Cardona, P. F. F. Carnelli, E. de Barbará, J. O. Fernández Niello, J. M. Figueira, D. Hojman *et al.*, in *Proceedings of the VIII Latin American Symposium on Nuclear Physics and Applications*, AIP Conf. Proc. No. 1265 (AIP, New York, 2010), p. 104.
- [44] L. Fimiani, J. M. Figueira, G. V. Martí, J. E. Testoni, A. Arazi, O. A. Capurro, W. H. Z. Cárdenas, M. A. Cardona, P. F. F. Carnelli, E. de Barbará *et al.*, *EPJ Web Conf.* **17**, 03003 (2011).
- [45] G. V. Martí, L. Fimiani, J. M. Figueira, J. E. Testoni, A. Arazi, O. A. Capurro, W. H. Z. Cárdenas, M. A. Cardona, P. F. F. Carnelli, E. de Barbará *et al.*, in *Proceedings of the IX Latin American Symposium on Nuclear Physics and Applications*, AIP Conf. Proc. No. 1423 (AIP, New York, 2012), p. 97.
- [46] J. Wilczynski and K. Siwek-Wilczynska, *Phys. Lett. B* **55**, 270 (1975).
- [47] D. Abriola, P. Carnelli, A. Arazi, J. Figueira, O. Capurro, M. Cardona, J. F. Niello, D. Hojman, L. Fimiani, P. Grinberg *et al.*, *Nucl. Instrum. Methods Phys. Res., Sect. B* **268**, 1793 (2010).
- [48] R. D. Woods and D. S. Saxon, *Phys. Rev.* **95**, 577 (1954).
- [49] I. J. Thompson, *Comp. Phys. Rep.* **7**, 167 (1988).
- [50] W. R. Leo, *Techniques for Nuclear and Particle Physics Experiments* (Springer, Berlin, 1987).
- [51] N. N. Deshmukh, S. Mukherjee, D. Patel, N. L. Singh, P. K. Rath, B. K. Nayak, D. C. Biswas, S. Santra, E. T. Mirgule, L. S. Danu *et al.*, *Phys. Rev. C* **83**, 024607 (2011).
- [52] M. E. Brandan and G. R. Satchler, *Phys. Rep.* **285**, 143 (1997).
- [53] G. R. Satchler and W. G. Love, *Phys. Rep.* **55**, 183 (1979).
- [54] K. H. Bray, M. Jain, K. S. Jayaraman, G. Lobianco, G. A. Moss, W. V. Oers, D. O. Wells, and F. Petrovich, *Nucl. Phys. A* **189**, 35 (1972).
- [55] M. F. Vineyard, J. Cook, K. W. Kemper, and M. N. Stephens, *Phys. Rev. C* **30**, 916 (1984).
- [56] L. C. Chamon, B. V. Carlson, L. R. Gasques, D. Pereira, C. De Conti, M. A. G. Alvarez, M. S. Hussein, M. A. Cândido Ribeiro, E. S. Rossi, and C. P. Silva, *Phys. Rev. C* **66**, 014610 (2002).
- [57] T. Udagawa and T. Tamura, *Phys. Rev. C* **29**, 1922 (1984).
- [58] T. Udagawa, B. T. Kim, and T. Tamura, *Phys. Rev. C* **32**, 124 (1985).
- [59] A. Gómez Camacho, P. R. S. Gomes, J. Lubian, E. F. Aguilera, and I. Padrón, *Phys. Rev. C* **76**, 044609 (2007).
- [60] A. Gómez Camacho, P. R. S. Gomes, J. Lubian, and I. Padrón, *Phys. Rev. C* **77**, 054606 (2008).
- [61] P. Frobrich and R. Lipperheide, *Theory of Nuclear Reactions* (Clarendon, Oxford, 1996).
- [62] P. R. S. Gomes, J. Lubian, I. Padron, and R. M. Anjos, *Phys. Rev. C* **71**, 017601 (2005).
- [63] J. Lubian, T. Correa, B. Paes, J. M. Figueira, D. Abriola, J. O. Fernández Niello, A. Arazi, O. A. Capurro, E. de Barbará, G. V. Martí *et al.*, *Nucl. Phys. A* **791**, 24 (2007).
- [64] J. Lubian, I. Padron, P. R. S. Gomes, A. M. M. Maciel, R. M. Anjos, S. B. Moraes, J. J. S. Alves, C. Muri, R. Liguori Neto, and N. Added, *Phys. Rev. C* **64**, 027601 (2001).